NTNU
Det skapende universitet

Måling av egenfrekvenser til sirkulær disk i luft og vann

Frode Kristoffer Kjøsnes

Master i energi og miljø
Innlevert: juni 2015
Hovedveileder: Pål Tore Selbo Storli, EPT
Medveileder: Torbjørn K. Nielsen, EPT
Petter Østby, Rainpower

Norges teknisk-naturvitenskapelige universitet
Institutt for energi- og prosessteknikk

NTNU
Norges teknisk-naturvitenskapelige universitet
Institutt for energi- og prosessteknikk

EPT-M-2015-43

MASTEROPPGAVE

for

Student Frode Kjøsnes

Våren 2015

Måling av egenfrekvenser til sirkulær disk i luft og vann

Measurement of natural frequencies in a circular disc in air and water

Bakgrunn og målsetting

Mange Francisturbiner i Norge er modne for utskifting etter å ha vært i drift i nærmere femti år. Flere Francisturbiner som har fått nye og «moderne» løpehjul har opplevd problemer knyttet til utmatting og skovlbrudd. Disse problemene tror man er grunnet at egenfrekvenser i løpehjulene har blitt for nære frekvenser som dukker opp under drift og man har kommet nærme å få resonans i løpehjulene. For enkle strukturer er det relativt lett å regne seg frem til strukturens egenfrekvenser. Når strukturene blir såpass komplekse som er Francis løpehjul som i tillegg er fylt med vann omringet av tynne sjikt med vann mot andre faste flater viser det seg mye vanskeligere å regne på, og teori stemmer ikke godt nok med praksis. Det er behov for å kunne bestemme egenfrekvensen til slike komplekse strukturer og dette behovet stammer fra ønsket om å kunne konstruere nye løpehjul som vil ha egenskaper som gir problemfri drift i nye femti år.

Det er blitt etablert et måleoppsett bestående av en instrumentert disk på Vannkraftlaben ved NTNU som har vært gjenstand for målinger som del av en masteroppgave. Eksperimentelt er det knyttet utfordringer til å måle hvilke egenfrekvenser en konstruksjon har og det foreligger flere forslag til forbedringer knyttet til å få gode målinger på det eksisterende oppsettet. Å få gode målinger er veldig viktig for å validere resultat fra simuleringsverktøy.

Oppgaven bearbeides ut fra følgende punkter

1 Litteratursøk angående strukturanalyse og strukturers egenfrekvenser
2 Gjøre nye og forbedrede målinger på eksisterende måleoppsett med de forslag til forbedringer som er blitt presentert
3 Forberede, og hvis tiden tillater det, å flytte måleoppsettet over til et modellhjul og gjennomføre målinger på hjulet nedsenket i vann

Senest 14 dager etter utlevering av oppgaven skal kandidaten levere/sende instituttet en detaljert fremdrift- og eventuelt forsøksplan for oppgaven til evaluering og eventuelt diskusjon med faglig ansvarlig/veiledere. Detaljer ved eventuell utførelse av dataprogrammer skal avtales nærmere i samråd med faglig ansvarlig.

Besvarelsen redigeres mest mulig som en forskningsrapport med et sammendrag både på norsk og engelsk, konklusjon, litteraturliste, innholdsfortegnelse etc. Ved utarbeidelsen av teksten skal kandidaten legge vekt på å gjøre teksten oversiktlig og velskrevet. Med henblikk på lesning av besvarelsen er det viktig at de nødvendige henvisninger for korresponderende steder i tekst, tabeller og figurer anføres på begge steder. Ved bedømmelsen legges det stor vekt på at resultatene er grundig bearbeidet, at de oppstilles tabellarisk og/eller grafisk på en oversiktlig måte, og at de er diskutert utførlig.

Alle benyttede kilder, også muntlige opplysninger, skal oppgis på fullstendig måte. For tidsskrifter og bøker oppgis forfatter, tittel, årgang, sidetall og eventuelt figurnummer.

Det forutsettes at kandidaten tar initiativ til og holder nødvendig kontakt med faglærer og veileder(e). Kandidaten skal rette seg etter de reglementer og retningslinjer som gjelder ved alle (andre) fagmiljøer som kandidaten har kontakt med gjennom sin utførelse av oppgaven, samt etter eventuelle pålegg fra Institutt for energi- og prosessteknikk.

Risikovurdering av kandidatens arbeid skal gjennomføres i henhold til instituttets prosedyrer. Risikovurderingen skal dokumenteres og inngå som del av besvarelsen. Hendelser relatert til kandidatens arbeid med uheldig innvirkning på helse, miljø eller sikkerhet, skal dokumenteres og inngå som en del av besvarelsen. Hvis dokumentasjonen på risikovurderingen utgjør veldig mange sider, leveres den fulle versjonen elektronisk til veileder og et utdrag inkluderes i besvarelsen.

I henhold til "Utfyllende regler til studieforskriften for teknologistudiet/sivilingeniørstudiet" ved NTNU § 20, forbeholder instituttet seg retten til å benytte alle resultater og data til undervisnings- og forskningsformål, samt til fremtidige publikasjoner.

Besvarelsen leveres digitalt i DAIM. Et faglig sammendrag med oppgavens tittel, kandidatens navn, veileders navn, årstall, instituttnavn, og NTNUs logo og navn, leveres til instituttet som en separat pdf-fil. Etter avtale leveres besvarelse og evt. annet materiale til veileder i digitalt format.

☒ Arbeid i laboratorium (vannkraftlaboratoriet, strømningsteknisk, varmeteknisk)
☐ Feltarbeid

NTNU, Institutt for energi- og prosessteknikk, 14. januar 2015

Olav Bolland
Instituttleder

Pål-Tore Storli
Faglig ansvarlig/veileder

Medveileder: Petter Østby, Rainpower
Torbjørn K. Nielsen, Vannkraftlaboratoriet

Preface

This master thesis was written at the Hydropower Laboratory at NTNU during the spring of 2015.

Prior to this thesis I had no knowledge about structural vibrations and little experimental experience. This spring has been an interesting journey and I have learnt a lot.

I would like to thank my fellow students for all the laughter and good times we have shared together. My supervisors have given good advices and guided me in the right direction, many thanks are given to them. Special thanks are given to Chirag Trivedi for the help he provided during the experiments.

Frode Kristoffer Amundsen Kjøsnes

Trondheim 15. June 2015

Summary

In this master thesis, the natural frequencies of a disk and a reversible pump turbine have been explored. The focus for the work has been to test how a nearby rigid surface influences these natural frequencies when submerged in water. The experiments produced good results for the disk, and the influence was determined. This was not the case for the turbine. The turbine tests were not able to identify the modes in water, and it was therefore not possible to determine the influence from a nearby rigid surface for the turbine.

Two methods of mode identification have been presented. The methods were able to identify some of the modes in air, but some of the modes had behaviour which can not be explained by these methods. Further research is needed to identify these modes.

Three methods of excitation have been tested, two of the methods use piezoelectric patches and the third was an impact excitation. They gave almost identical results, the largest deviation observed was only 1 Hz. Impact excitation was shown to be the most time efficient method. Improvement proposals for the hammer have also been presented.

Sammendrag

I denne oppgaven har egenfrekvensene til en sirkulær plate og en reversibel pumpeturbin blitt utforsket. Det har blitt testet hvordan de endrer seg i vann med fokus på hvordan avstanden til en stiv overflate påvirker egenfrekvensene. Forsøkene ga gode resultater for platen, og påvirkningen fra en nærliggende stiv overflate ble kartlagt. Forsøkene ga derimot ikke gode resultater for turbinen. Eksperimentene klarte ikke å identifisere de forskjellige egenfrekvensene i vann, og det var derfor ikke mulig å avdekke påvirkningen som en nærliggende stiv overflate har på turbinen.

To metoder for å identifisere egenfrekvensene er presentert. Ved å bruke disse ble noen av egenfrekvensene til turbinen avdekket i luft. Det oppstod noen egenfrekvenser som ikke lot seg forklare, og det er nødvendig med videre forskning for å identifisere disse.

Tre eksiteringmetoder ble testet. To av metodene brukte piezoelektriske lapper og i den tredje ble det brukt en hammer for å eksitere. Alle tre metodene ga nesten identiske resultater, avviket mellom dem var på kun 1 Hz. Å eksitere med hammer

viste seg å være mest praktisk for slike forsøk. Forslag for å forbedre hammeren er presentert.

Contents

List of Figures

List of Tables

Nomenclature and abbreviation

c	Damping	[Ns/m]
D_m	Runner inlet diameter	[m]
f	Frequency	[Hz]
F_s	Sample frequency	[Hz]
h_1	Normalized distance to water surface	[-]
H_1	Distance to water surface	[m]
h_2	Normalized distance to a rigid surface	[-]
H_2	Distance to a rigid surface	[m]
h_D	Disk thickness	[m]
k	Number of nodal diameters	[-]
$\hat{k}$	Spring constant	[N/m]
m	Mass	[kg]
n	Harmonic index	[-]
r	Radius	[m]
w	Window function	[-]
X_k	Vibration of a mode having k diametrical nodal lines	[-]
Z_g	Number of guide vanes	[-]
Z_r	Number of runner blades	[-]
$\Delta\alpha$	Phase shift between two accelerometers	[rad]
λ	Added mass factor	[-]
ρ	Density	[kg/m^3]
$\Delta\theta_{spatial}$	Spatial phase angle between two accelerometers	[rad]
ζ	Damping ratio	[-]
FFT	Fast Fourier Transform	
FRF	Frequency Response Function	
FRR	Frequency Reduction Ratio	
ND	Nodal Diameter	

Introduction

High head hydraulic turbines have in recent years experienced vibration problems due to changed operation conditions. These problems manifest them self in either high noises or increased fatigue, which leads to cracks in the material and eventually rupture. The operating conditions have changed in the last 25 years in Norway, from turbines running for a long period of time uninterrupted to turbines being stopped and started many times a day. Under start up and shut down turbines are likely to experience forces with frequencies matching the natural frequency of the runner. This creates resonance which is believed to be the main cause for the increased fatigue. It is important to be able to predict these frequencies.

Calculating the natural frequencies of the runner is complex, since it is not only depending on the geometry and material properties of the turbine. It is also a function of the boundary conditions, like; surrounding fluid, rotation, distance to rigid surfaces, flow conditions, vibration mode shape and vibration amplitude. Numerical simulations need to take into account these effects. Experimental data is required to validate and improve the numerical calculations. This work is a small contribution to the validation basis needed.

1 Literature study

The following is a summary of the most important publications concerning structural vibration having focus on turbines and plates.

Yuji Kubota et al. published a paper called *Vibration of Rotating Bladed Disc Excited by Stationary Distributed Forces* in 1983 [5]. This paper is one of the first to provide analytical equations to estimate the vibrations and deflection caused by the Rotor-Stator interaction (RSI), this lead to the *exciting condition*. Experiments were conducted to verify his assumptions. He found that resonance will not occur if the *exciting condition* is not met, even if the natural and exciting frequencies coincide. He looked exclusively on diametrical mode shapes. The *exciting condition* is show in eq 1, and will is discussed in section 2.2.1.

$$nZ_g \pm k = mZ_r \quad [-] \tag{1}$$

Tanaka H. studied, in 1990, the vibrations and stresses on a high head reversible pump turbines [6]. A scaled model were used in the experiments. The paper covers a broad spectre of interesting factors that influence the runner vibration, like: axial distance between head cover and runner, runner seal clearance, radial distance between guide vanes and runner blades, phase difference between crown and band, and details how to scale a runner for modal testing.

In 2006 C.G. Rodriguez did an experimental investigation on the added mass effect on a Francis runner submerged in still water [2]. He suspended the runner with a rope into a tank filled with water, where he preformed several impact test to obtain the added mass and added dampening for the turbine. In his studies he found a non dimensional submergence depth for where the the added mass is stable, and that the affect from the added damping from water, on the natural frequency, is neglectable in comparison with the added mass.

In 2008 X. Escaler et al. presented, under the 24th Symposium on Hydraulic Machinery and Systems, his paper *Experimental Modal Analysis of a Francis Model Runner* [14]. They studied the natural frequencies of the runner both in air and water. They excited the turbine using an impact hammer, and found that the added mass increased considerably along with the number of nodal diameters. His main results are presented in table 1. The frequency reduction ratio, $\frac{f_{water}}{f_{air}}$, varied from 0.71 for 2ND to 0.36 for 7ND. In other words the largest frequency reduction was 64%.

Table 1: Main results from X. Escaler

Shape	Frequency [Hz]		FRR[1]
	Air	Water	f_{water}/f_{air}
0ND	658	568	0,86
1ND	1056	643	0,61
2ND	511	365	0,71
3ND	801	420	0,52
4ND	869	404	0,46
5ND	965	383	0,40
6ND	979	365	0,37
7ND	989	355	0,36

In 2014 David Valentin et al. published a paper on disk vibrations [1]. He did a thorough study on how the added mass and dampening is effected by the boundary conditions. He used an experimental and numerical approach to investigate this. His studies are limited to plates. The added mass were studied with varying distances to a rigid surface, both in axial and radial direction. The main results are presented in figure 1. His experiments show that the added mass is larger for the modes with few nodal diameters. This is contradicting to what X. Escaler found in 2008. Plates and turbines therefore have different behaviour.

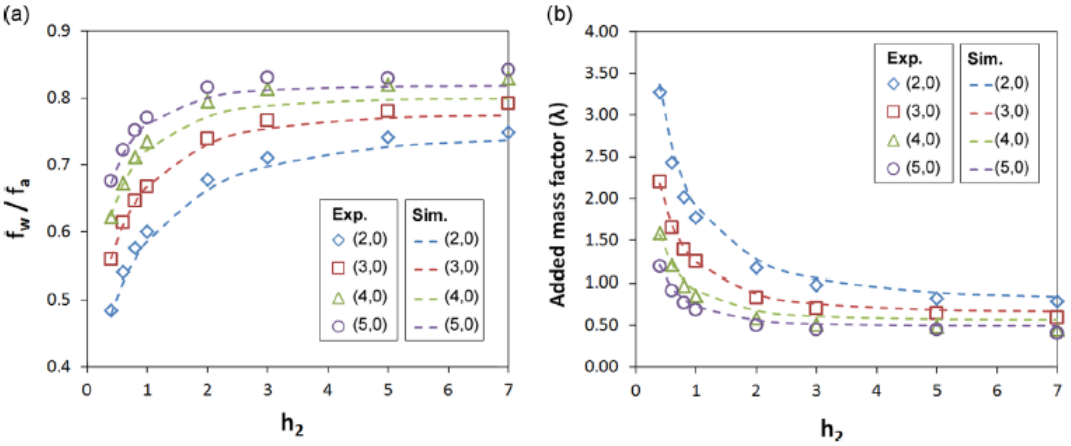

Figure 1: Effect from nearby rigid surface. Where h_2 is the distance to a rigid surface normalized against the disk thickness.

[1]Frequency Reduction Ratio (FRR) is the ratio between a natural frequency in water over the natural frequency in air.

In 2015 A. Presas et al. studied the effect rotation has on the natural frequencies [16]. They conducted experiments, on a rotating disk in air and water, and compared the results with an analytical model. Their main finding was that rotation is almost negligible when the surrounding fluid is air, but is important to consider when the fluid is dense, i.e. water. From a stationary reference point will a natural frequency measured with no rotation be transformed into two natural frequencies when measured with rotation. The frequency distance between the peaks increases with increasing rotational speed.

2 Theory

This chapter gives a rough introduction to the nature of structure vibrations. The theory will cover the basics of circular plate vibration. Analytical solutions for a whole turbine does not exist due to the complex geometry of the object. Numerical methods are necessary to solve systems like that.

2.1 Natural frequencies and resonance

The natural frequencies of an object are the frequencies the object will vibrate at if there is no external forces acting on the object. All objects have unique natural frequencies. If an external force is applied to an object it will vibrate with the same frequency as the external force [4]. If the frequency of the external force coincide with the natural frequency of the object, it will increase the vibration amplitude multiple times, and decrease the life of the object. This is known as resonance.

The equation (2) describing the fundamental simple mass-spring system gives a good foundation for understanding the behaviour of vibrations.

$$my'' + cy' + \hat{k}y = 0 \quad [N] \tag{2}$$

Here m is the mass of the system, c is the damping and $\hat{k}$ [2] is the spring constant. This equation was solved a long time ago together with the natural frequency.

$$f_{vacuum} = \frac{1}{2\pi}\sqrt{\frac{\hat{k}}{m}} \quad [Hz] \tag{3}$$

The frequency is determined by the mass and stiffness. This solution holds for simple undamped systems with one degree of freedom, but do not take the ambient fluid into account, which will contribute with added mass and damping.

2.1.1 Added mass

If an object is accelerated relative to a surrounding fluid it appears to have an additional mass. This is known as added mass, and is a key factor to consider for turbine designers. To account for the added mass designers previously relied on "rules of thumbs" [11], which were grounded on experimental experience. In

[2] A hat is used to set it apart from the number of nodal diameters.

recent years a combination of CFD and FEM has become the "state of the art" for calculating the added mass [10].

It is a complex task to analytically predetermine the added mass of an object, because it is a function of body geometry, mode-shape, submergence, nearby rigid structures, vibration amplitude and flow conditions [2].

A vibrating object immersed in a fluid has to move the surrounding fluid, and this adds an additional mass to the object, m_A. Since all fluids are viscous, some of the energy will be dissipated. This effect adds an extra dampening coefficient, c_A, to equation (2). These effects are barely noticeable in fluids with low density and viscosity, such as air, but will have a large influence in denser and more viscous fluids like water. Added mass can lower the natural frequencies by 64 % in extreme cases, referring to table 1.

The fluid force, F_{fluid}, acting on a vibrating object is mainly created by the pressure drag. This force can be expressed by the Navier-Stokes equations if the fluid is considered to be incompressible, newtonian and if the nonlinear terms are neglected [1]. Introducing the fluid force in equation (2) leads to the following equation:

$$my'' + cy' + \hat{k}y = F_{fluid} = -m_A y'' - c_A y' \quad [N] \tag{4}$$

Rearranging gives:

$$(m + m_A)y'' + (c + c_A)y' + \hat{k}y = 0 \quad [N] \tag{5}$$

This leads to the following expression for the undamped natural frequency:

$$f_{fluid} = \frac{1}{2\pi}\sqrt{\frac{\hat{k}}{m + m_A}} \quad [Hz] \tag{6}$$

Frequencies are lowered due to the inertia of the water. There is also a reduction contribution from the damping:

$$f_d = f_{fluid}\sqrt{1 - \zeta^2} \quad [Hz] \tag{7}$$

where: ζ is the damping ratio, and f_d is the damped natural frequency. The value of ζ can be determined experimentally by equation 8, where the frequencies f_B and f_A, whose amplitudes correspond to half the power (-3 dB) of the frequency response function (FRF) at $f = f_d$ [2], see figure 2.

$$\zeta = \frac{f_B - f_A}{2f_d} \quad [-] \tag{8}$$

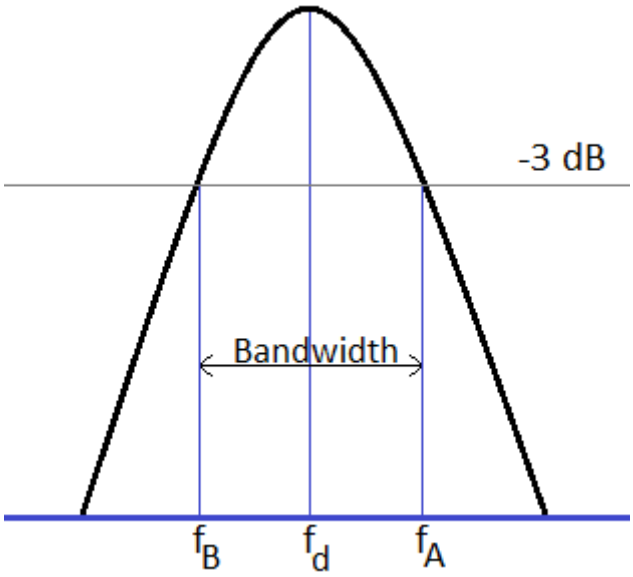

Figure 2: Half power bandwidth.

The frequency reduction ratio (FRR) and added mass factor λ are two commonly used values to quantify the added mass.

$$\lambda = \frac{m_A}{m} = \left(\frac{f_a}{f_f}\right)^2 - 1 \quad [-] \tag{9}$$

$$FRR = \frac{f_{water}}{f_{air}} \quad [-] \tag{10}$$

2.1.2 Nearby rigid structures

The presence of a rigid surface influences the natural frequencies as seen in figure 1. If the distance from a vibrating object to a rigid surface decreases the added mass will increase, thus lowering the natural frequency. This happens because the wall surface imposes velocity constraints on the water, both the no slip constraint and no normal velocity component.

Y. Kubota and T. Suzuki provided a simple model to calculate the added mass for diametrical modes on an annular disk [9]. In equation (11) λ represent the added mass factor, ρ the density, h_D disc thickness, k the number of nodal diameters, $r_0 = \sqrt{r_{inner} r_{outer}}$ the average radius, H_1 distance between the plate and water

surface and H_2 the distance between plate and a rigid surface. These equations are only valid for $k > 0$ and for r_0 where no nodal circles are present [1].

$$\lambda(H_1, H_2) = \frac{\rho_f r_0}{k \rho_D h_D} \left[\tanh\left(\frac{k}{r_0} H_1\right) + \coth\left(\frac{k}{r_0} H_2\right) \right] \quad [-] \tag{11}$$

The presence of nearby rigid structures lowers the natural frequencies. Valentin showed in his paper that both the axial and radial distance to a rigid surface influences the added mass effect[1]. Decreasing the distance increases the added mass effect. The radial contribution is not taken into account in equation (11).

2.1.3 Mode shapes

There are several different ways a structure can vibrate: torsional (twisting), flexural (bending) and translational (dilatation and compression). Translational and torsional vibrating will not be presented here, since it is not believed that these modes are the main cause of the vibration problems.

When a system is excited it will not just vibrate with one frequency, it will vibrate with infinite many frequencies [6]. Each frequency corresponds to an unique mode shape. Flexural mode shapes are defined by nodal lines, these are lines with zero deflection. There are two fundamental types of nodal lines for plates: the circular and the diametrical lines. An example of nodal diameters can be seen in figure 3. Vibration patterns with circular nodal lines have typically higher natural frequencies than those without [8]. They are therefore less likely to be excited under operation, and are therefore of less interest for an engineer.

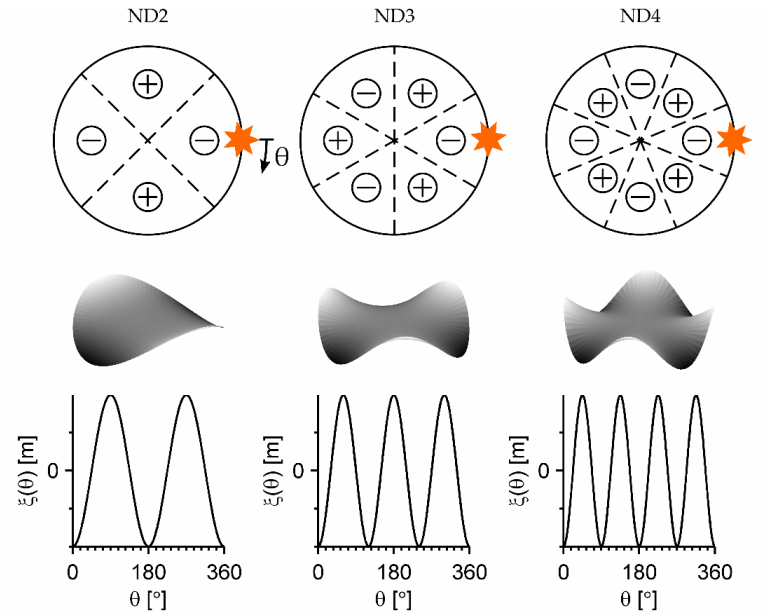

Figure 3: Nodal diameters [7].

2.2 Rotor-Stator Interaction and Fatigue

After each guide vane there is a wake with lower velocity, thus higher pressure, than the surrounding water. When a runner blade passes this wake it experience rapid pressure fluctuations. This effect is known as the Rotor-Stator interaction (RSI), and is the main source of turbine excitation for high head turbines.

The RSI frequency is calculated by:

$$f_r = n \cdot Z_g \cdot f_n \quad [Hz] \tag{12}$$

Where f_r is the RSI frequency, Z_g is the number of guide vanes, f_n is the rotational speed of the runner and n is the n-th harmonic order of vibration. Resonance will occur if the natural frequencies of the runner coincidence with these frequencies, given that the *exciting condition* is met, ref. section 2.2.1.

2.2.1 Theoretical calculations

When an external force is applied to the runner, it will vibrate with the same frequency as the exciting force. The RSI is the main contributor for external

forces.

Kubota and Tanaka provided equations, for diametrical modes, to calculate the vibration deflection induced by the RSI, in [5] and [6].

$$f_r = n \cdot Z_g \cdot f_n \quad [Hz] \tag{13}$$

$$X_k = \frac{A}{2}\Bigg(C_1 \sin\left[(2\pi f_r t - k\phi) + \pi(Z_r - 1)\frac{(nZ_g + k))}{Z_g}\right] + C_2 \sin\left[(2\pi f_r t + k\phi) + \pi(Z_r - 1)\frac{(nZ_g - k))}{Z_g}\right]\Bigg) \quad [-] \tag{14}$$

where:

$$C_1 = \frac{sin\big(\pi(nZ_g + k)\big)}{sin\left(\frac{\pi(nZ_g+k)}{Zr}\right)} \quad [-] \tag{15}$$

$$C_2 = \frac{sin\big(\pi(nZ_g - k)\big)}{sin\left(\frac{\pi(nZ_g-k)}{Zr}\right)} \quad [-] \tag{16}$$

The numerators in constants C_1 and C_2 are zero, since $nZ_g \pm k = integer$. Therefore there will be no vibration unless the denominator are also zero. This gives us the *exciting-condition*. Where m is an arbitrary integer and k is the number of nodal diameters in the vibration.

$$nZ_g \pm k = mZ_r \quad [-] \tag{17}$$

When equation 17 is fulfilled the values of $C_1, C_2 = \pm Z_r$, the equation for deflection becomes:

$$X_k = \frac{AZ_r}{2}\big(\sin(2\pi f_r t - k\phi) + \sin(2\pi f_r t + k\phi)\big) \quad [-] \tag{18}$$

The consequences of eq.(17), the exciting condition, is remarkable. It states that resonance will not occur even if the exciting frequency is equal to the natural frequency, unless the equation is fulfilled. This was proved in [5].

For example: There are 28 guide vanes in our laboratory francis rig and the reversible-pump turbine has 6 runner blades. With this configuration it is impossible to excite mode shapes with an odd number of nodal diameters, since m and n are integers.

2.3 Excitation

The following excitation methods are utilized in this study.

Impact excitation
Applying a short force impulse to a system will excite all natural frequencies and mode shapes. If a hammer is used, it is important that is has a hard tip. The excited frequency range will be wider as the hardness of the hammer tip is increased [12].

Noise excitation
This method continuously excite all frequencies with the same amplitude.

Sweep excitation
This is a continuous signal which start at one frequency and continuously increases the frequency until it reaches the end frequency.

Stepwise sweep excitation
This differs from sweep excitation since it increases the frequency stepwise instead of continuously.

2.4 Measurement and processing

2.4.1 Sampling rate

According to Nyquist–Shannon's sampling theorem the sampling frequency have to be larger than twice the frequency measured, $F_s > 2f$. This is done in order to avoid alias frequencies [3].

In this thesis the dynamic signal acquisition module NI-9233 is used to log the measurements. This module has limitations in its sampling frequency (Fs), only certain values for Fs is acceptable. These values are determined by equation (19), where $f_m = 12.8$ MHz.

$$for\ F_s \leq 25.65\ kS/s$$
$$Fs = \frac{f_m}{256n},\ n = 2, 3, ..., 25 \tag{19}$$
$$for\ F_s > 25.65\ kS/s$$
$$Fs = \frac{f_m}{128n},\ n = 2, 3 \tag{20}$$

The module automatically corrects the sampling frequency if it does not satisfy the above equations. It chooses the nearest higher value for Fs in order to avoid aliasing. It is important to be aware of this since a wrong sample frequency value will give a wrong time step between data points, which in turn will lead to incorrect frequencies in the frequency domain when preforming Fourier transformations (FFT).

2.4.2 Dimaterical mode identification

Phase difference
The phase shift between two sensors which is placed on the same radius, can be used to determine the mode shape. The mode shape is determined by the spatial angle between the sensors and phase shift [16], see equation (21). This method is only valid for diametrical modes.

$$k = \frac{\Delta\alpha}{\Delta\theta_{spatial}} \quad [-] \tag{21}$$

where k is the number of diametrical lines, $\Delta\theta_{spatial}$ is the spatial angle between the sensors and $\Delta\alpha$ is the phase shift between the sensors.

Impact method
The positions of nodal lines are determined on the excitation location. Impacting an object all around its circumference will make each nodal line pass a reference point exactly two times. If an accelerometer is placed at this reference point, it will be passed by four nodal lines for a 2ND mode. Using FFT on the measurements from all impact points gives the frequency spectrum. Since natural frequencies do not change with impact location, it is possible to identify a mode shape from the amplitude variations along the impacts given a constant excitation force. Plotting the amplitude against the impacts for a given mode will result in a sinusoidal curve. The number of valleys is twice the number of nodal lines. The valleys will not have zero amplitude, since the nodal lines are infinitesimal whereas the accelerometers are not. This method is only able to detect diametrical modes.

2.4.3 Spectral leakage and windowing

All Fourier transforms, like FFT, assumes that the sampled data is periodic, and continuous at the beginning and the end. If the data is not, a smearing of its

spectrum will occur when it is transformed into the frequency domain. This is known as leakage[13].

Windows reduces the spectral leakage by forcing the samples to be periodic by multiplying each sample element with the window function. There are many different windows, all with their own area of application. If a sample is already periodic, then windows actually generates more leakage. Below is a description of the two used windows in this thesis.

Hanning

The most common and widely used window is the Hanning window. This window works very well if the signal is composed of several sine waves. This window is applied on measurements done by sweep and noise excitations. The definition is seen below and an illustration is shown in figure 4.

$$w(n) = 0.5\left(1 - \cos\left(\frac{2\pi n}{N-1}\right)\right) \quad [-] \tag{22}$$

where $n = 0, 1, \ldots, N-1$, N is the length of the sample and $w(n)$ is the window value.

Exponential

This window is appropriate for analysing decaying transient responses which are longer than the window. This window adds artificial damping on all modes ensuring that the periodicity is reached.

$$w(n) = e^{\frac{n\ln(f)}{N-1}} = f^{\frac{n}{N-1}} \quad [-] \tag{23}$$

where $n = 0, 1, \ldots, N-1$, N is the length of the sample, f is the final value and $w(n)$ is the window value.

If the response signal in an impact test decays to zero (or near zero) before the end of the sampling window, there will be no leakage, and no special windowing is required [13].

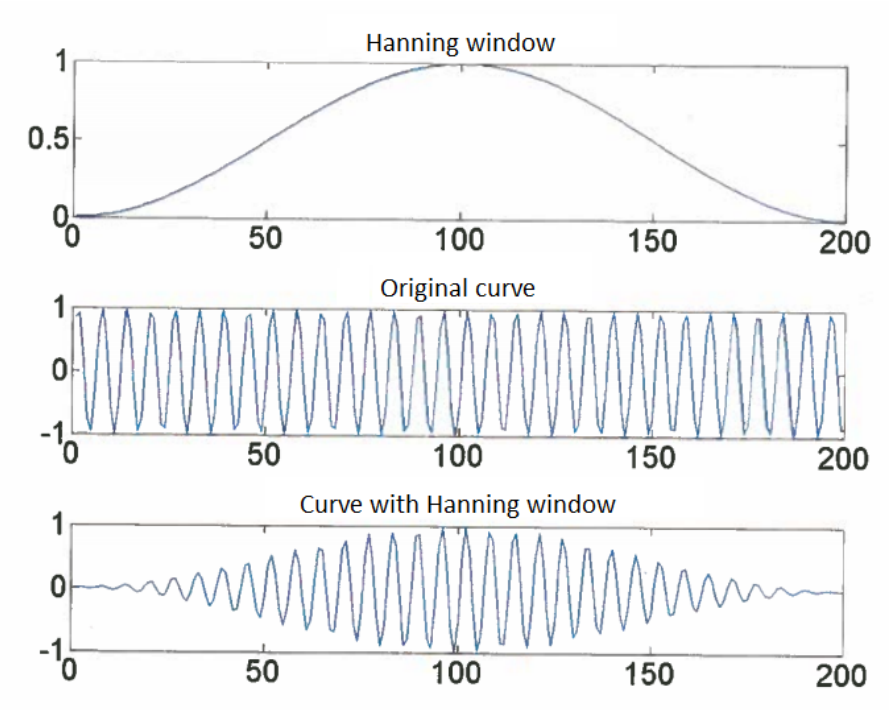

Figure 4: Illustration of the Hanning window [18].

2.4.4 Frequency Response Function

Frequency Response Functions (FRF) describes how systems respond to excitations, they are basically the same as FFTs. A FRF is made up by two signals: the stimulus and the response signals. The FRF is the ratio between the response signal and stimulus signal, where the response and stimulus signals are in the frequency domain.

3 Method

3.1 Experimental setup and instrumentation

The accelerometers used in the experiments are the Dytran 3006A They are very light, so the mass is assumed to have a negligible influence on the frequencies. They are mounted to the disk by screws, but glued on the pump turbine in order not to damage the turbine.[3] The sensor signals are collected by a National Instrument (NI) 9233 module.

A piezoelectric patch P-876.A15 is glued to the plate using an strong epoxy adhesive. This patch has an operating range from -250 V to 1000 V. A NI 9263 module is used to generate the voltage signal, this module can generate electrical signals with amplitude of -10 V to 10 V. The signal is amplified with a voltage amplifier (E-385 DuraAct Piezo driver Module) which has a voltage gain of 25. A NI 9239 module monitors the output from the amplifier.

The modules are connected to a computer through a cDAQ-9172 chassis. The signals are later processed in LabView.

3.1.1 Plate

The experimental rig is the same that was used in [7], only with a slight modification. In order to investigate the added mass the plate was equipped with a new threaded shaft, allowing for distance variation between the plate and the bottom of the tank. The accelerometer was placed at the outer rim of the plate, and the piezoelectric patch was placed between the accelerometer and the shaft. The patch has to be placed on the same θ-coordinate ($\pm 180°$) as the accelerometer in order to ensure that all nodal modes are excited.

The investigation started in air to find the most suitable and efficient method of excitation. The stepwise sweep, noise and impact excitation methods were tested. Averaging the results will reduce the random uncertainties, so each excitation is repeated five times each. The program that generates the stepwise sweep signal is constructed in such a way that each frequency is sent for one second before it

[3] The accelerometers are placed in the outlet of the blades. The blades are very thin, so it would be nearly impossible to repair the blades if holes were drilled in order to mount the accelerometers.

increments. Noise excitation has non of these constrains, and can be run for a short time. The sample frequency (F_S) for each method is 5000 Hz, and the logging times for sweep, noise and impact are 22 minutes[4], 60 seconds and 8 seconds respectively.

To investigate how the added mass changes with distance (H_2) to a rigid surface, the plate is impacted eight times for each value of H_2 to ensure good average results. Impact excitation were chosen on basis of the experimental results obtained in air, see section 4.1.1 and 5.1.1. The depth (H_1) is kept constant during the test in order to isolate the effects from H_1. The depth is chosen to be $H_1 = 16\ cm$, since the added mass contribution from depth is stabilized at this value [1]. A hole in the plate was drilled and the accelerometer was fixed with a screw.

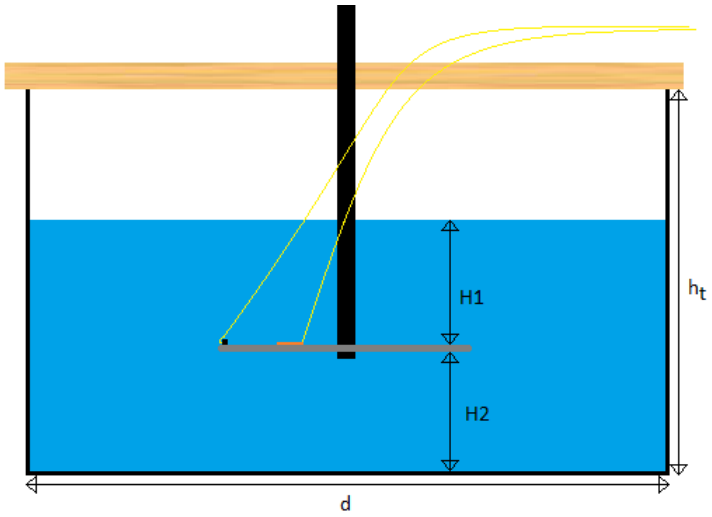

Figure 5: Drawing of the test rig.

Table 2: Test rig parameters

Parameter	Variable	Value [mm]
Disc outer radius	r_{outer}	250
Disc inner radius	r_{inner}	20
Disc thickness	h_D	20
Tank diameter	d	800
Tank height	h_t	490

[4]Excited frequency range: 400 Hz - 1700 Hz, this results in 1300 seconds which are ca 22 minutes.

3.1.2 Turbine

Two accelerometers are glued on the outlet of two neighbouring blades, see figure 6a. This was recommended after discussions with co-supervisor Petter Østby. It is believed that the blades will have the largest deflection, and this will make it easier for the sensors to measure the vibration. By using two accelerometers it is possible to use the *Phase difference method* to identify the mode shapes, see section 2.4.2 for justification. The turbine has 6 blades, so the spatial angle ($\Delta\theta_{spatial}$) between them is 60°.

The turbine must be excited around its circumference to enable the *impact method* of mode detection. Sweep excitation would be too cumbersome since the piezo-electric patch must be glued in order to work, and impact excitation is therefore the only viable option left. A simple rig was built in order to drop the hammer from a constant height, ensuring constant impact force during the test, see figure 6b. The hammer do not impact the turbine directly, it hits a mandrel which in turn excite the turbine. A mandrel has to be used since the hammer tip is very wide and soft. The mandrel is able to excite a wider frequency range and makes it easier to control the impact location.

An improvised impact hammer was made by gluing a third accelerometer to the back end of a hammer, see figure 6b. If it works properly it might negate the need to impact the turbine with a constant force, since the response signal can be normalized against the stimulus signal by creating a FRF-curve.

The runner dimensions and properties are summarized in table 3. The runner was designed by former PhD Grunde Olimstad [17].

Table 3: Reversible pump turbine characteristics

Parameter	Value		Material[5]	$CuAl_{10}Fe_5Ni_5$	
Inlet diameter	0,631	[m]	Density	7850	$[kg/m^3]$
Outlet diameter	0,349	[m]	Young's Modulus	110-115	[GPa]
Inlet height	0,059	[m]	Poisson's ratio	0,3	[-]
Number of blades	6	[-]			
Q^*_{ed}	0,133	[-]			
N^*_{ed}	0,223	[-]			
n^*	10,8	[Hz]			

[5]The material properties was given by the turbine manufacturer, since it was not included in [17].

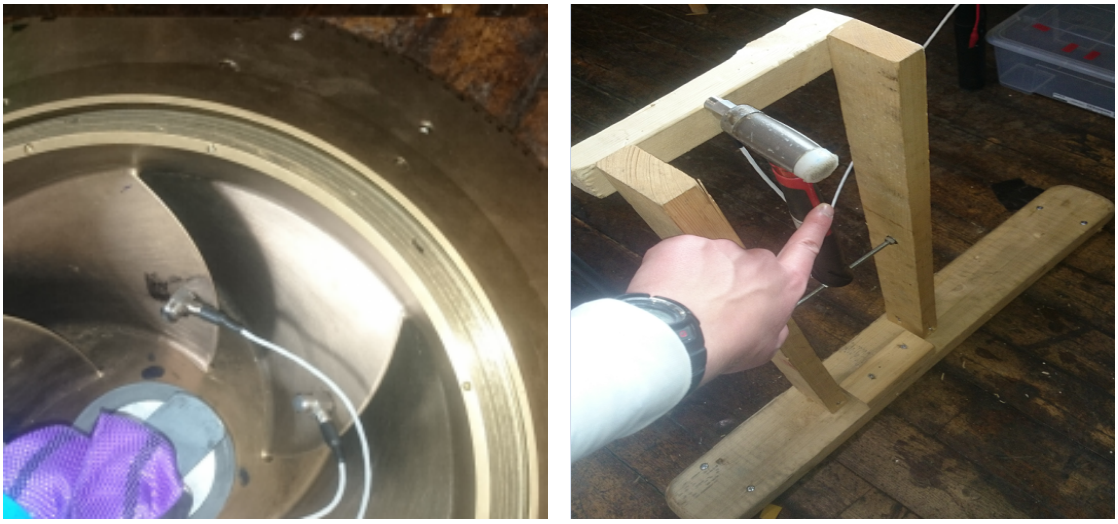

(a) Accelerometer position **(b)** Hammer rig

Figure 6: Experimental setup

Air

The turbine is suspended in air with a rope. The natural frequency of the rope is very low compared with the turbine and therefore the support will have an imperceptible effect on the runner response. The runner is excited with 171 equally spaced impact points around the circumference.

Water

When analysing the results from the impact tests done in air, it was revealed that the impact hammer did not work properly. It is therefore not possible to identify mode shapes with the *impact method* without exciting the turbine with a constant force. Several different new rigs were built in order to get constant impact force, but non were able to satisfactorily excite the runner. The walls of the tank made it difficult to get a clean impact on the turbine. A better rig could of course have been built, but time did not allow for it.

The turbine was instead impacted 21 times[6] at the same spot on the opposite side of the accelerometer. These impacts gave a phase difference and a response curve.

The turbine was submerged in water suspended with a rope. The distance from the water surface down to the turbine was chosen to be 12 cm according to C.G

[6]This is way more than necessary.

Rodriguez et al. This distance is sufficient to have a stable added mass, $H_1/D_m = \frac{12cm}{63.1cm} = 0.19 > 0.17$ [2]. The distance H_2 from the bottom of the tank to the turbine was 6.5 cm. It was planned to study the added mass as a function of H_2, but this was not done since it was not possible to identify the mode shapes. This is discussed in section 5.2.2.

4 Results

4.1 Plate

In the following sections the values of H_1 and H_2 have been normalized against the plate thickness h_d.

4.1.1 Sweep, noise and impact excitation

Two test were conducted on the plate with the same setup, one with stepwise sweep and one with noise. Additionally tests with a hammer were carried out in order to see how impact excitation compared with sweep and nose excitation. The results are presented in figure 7 and in table 4.

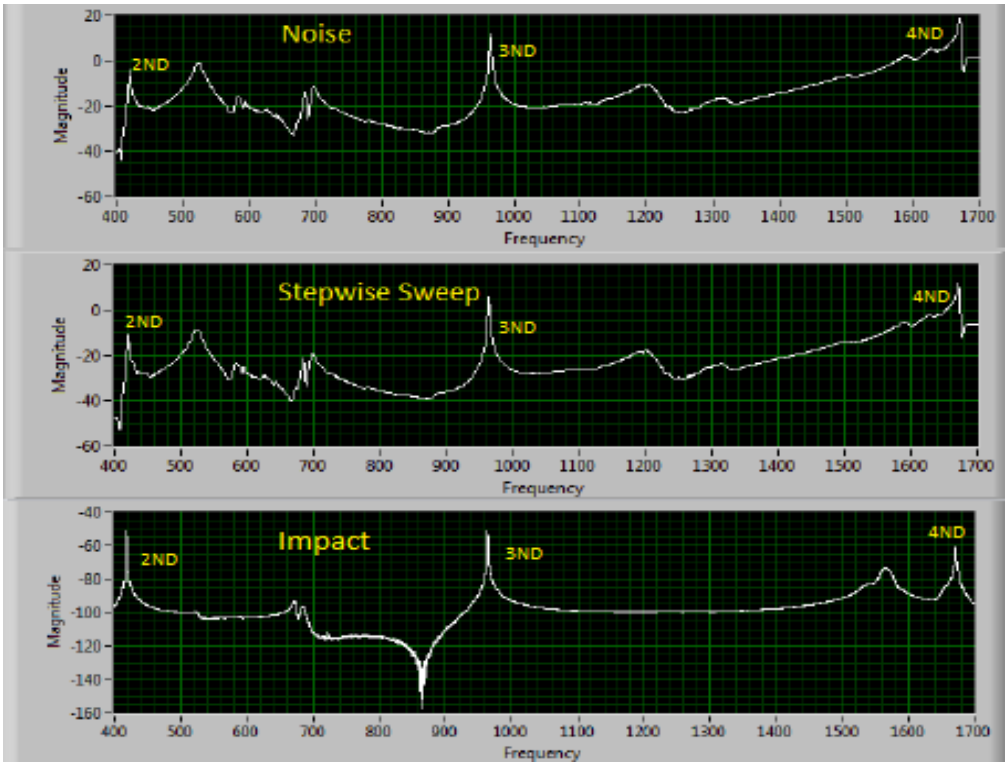

Figure 7: FRF for noise and stepwise sweep, while the impact excitation is a FFT. The experiment is done in air.

The curves for sweep and noise are identical in all manners, apart from a constant magnitude difference. Any differences seen in the figure are due to poor image

Table 4: Frequencies from each excitation method

Method [Hz]	2ND	3ND	4ND
Noise	417	964	1673
Stepwise sweep	417	964	1673
Impact	418	964	1672

quality.

4.1.2 Added mass affected by distance to a rigid surface

Experiments were carried out to see how the added mass changes with the distance to a rigid surface. Results can be found in table 5 and figures 8 and 9. The results are compared with the analytical equation (11).

Table 5: Results from test compared with calculated frequencies

h2	2ND [Hz]		3ND [Hz]		4ND [Hz]	
[-]	Experiment	Calculated	Experiment	Calculated	Experiment	Calculated
0,38	not tested	233	not tested	675	not tested	1313
0,50	263	261	635	727	1310	1382
0,75	275	279	672	758	1356	1419
1,00	294	301	719	792	1402	1457
1,50	317	313	766	809	1419	1475
2,00	328	327	774	825	1426	1490
2,50	334	333	778	831	1427	1494
3,00	346	337	790	834	1439	1496
3,50	336	339	792	835	1432	1497
4,00	337	340	789	836	not observed	1497
4,50	345	340	777	836	not observed	1497
5,00	343	341	785	836	not observed	1497
Air	417	-	964	-	1671	-

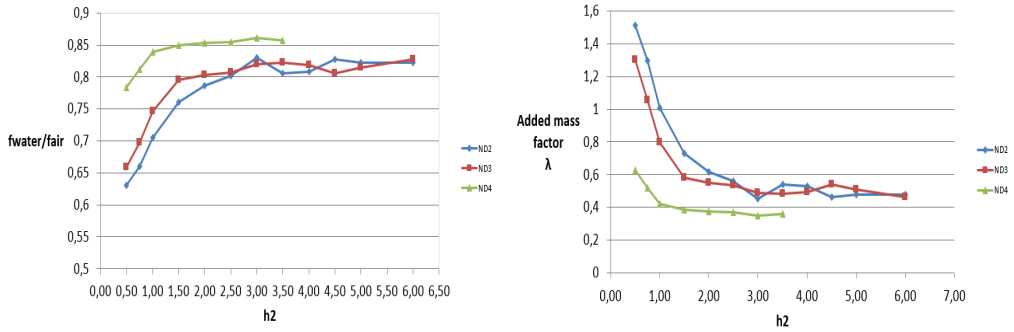

(a) Frequencies in water divided by air frequency

(b) Added mass factor $\lambda(h_2)$

Figure 8: Added mass as a function of h_2

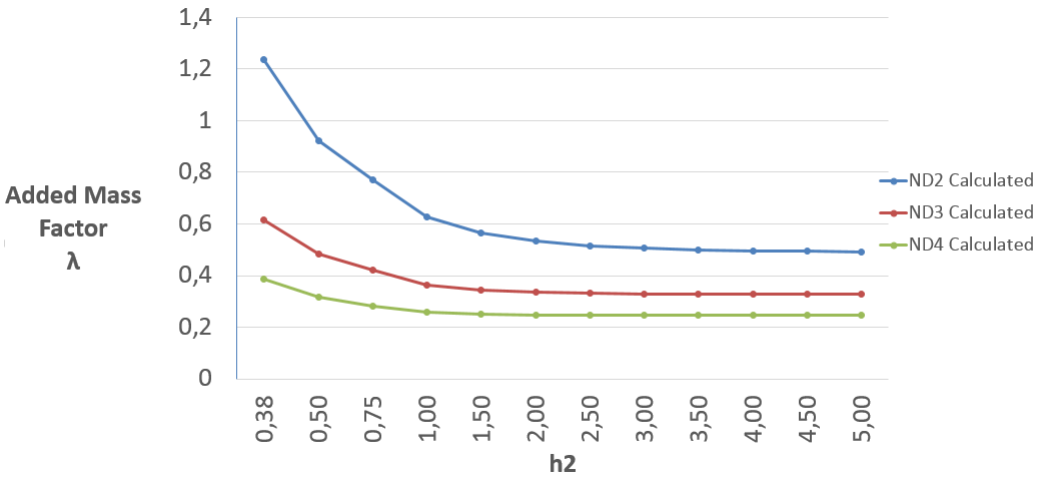

Figure 9: Added mass factor λ using eq. (11). The value $h_2 = 0.38$ is included in the calculations, but not in the experiments.

4.2 Reversible pump-turbine

4.2.1 Mode shape determination

The turbine was excited with 171 hammer blows around the perimeter with a constant force. The FFT is created in LabView, with an exponential window on the accelerometer.

All tests are conducted with a sample rate of 6250 Hz on each accelerometer and a logging time of 8 seconds. A rather long logging time was chosen to let the

vibration die out. This reduces the spectral leakage, referring to section 2.4.3.

All FFT-curves are plotted in figure 10. The equivalent electrical noise floor of the Dytran 3006A accelerometer is -100 dB. This is why the amplitudes are not smooth below -100 dB.

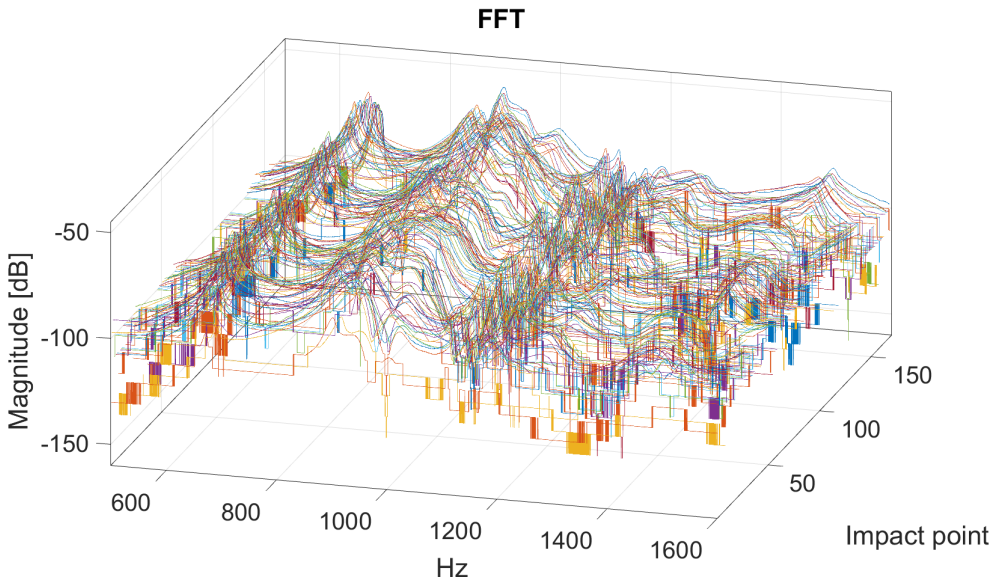

Figure 10: All impact points and their FFT

The different modes are better shown by taking the average of all impact curves and condensing them into one graph, see figure 12. The mode shapes are not yet identified. The amplitude of each impact point corresponding to the frequency of each peak in figure 12 is plotted in order to identify the mode shape. The results are shown in the figure 13.

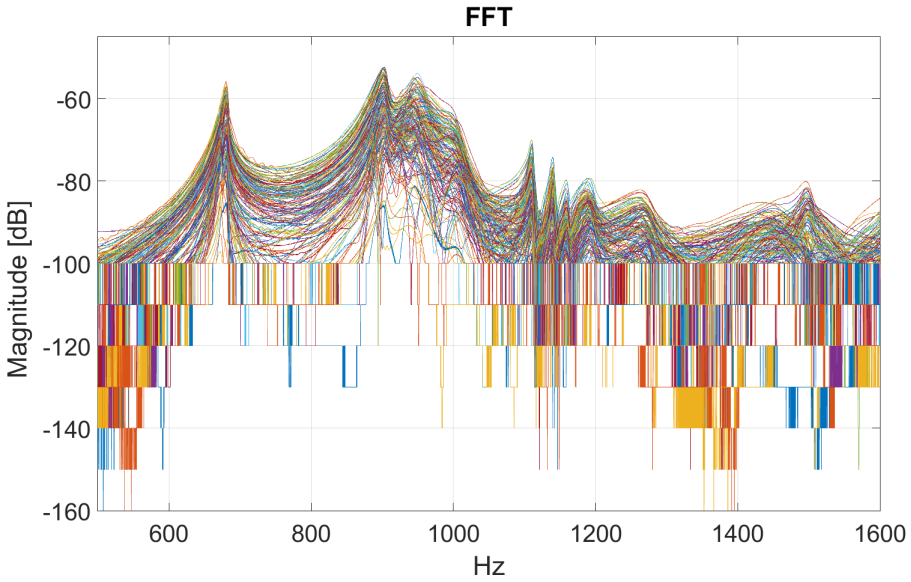

Figure 11: All impact points and their FFT

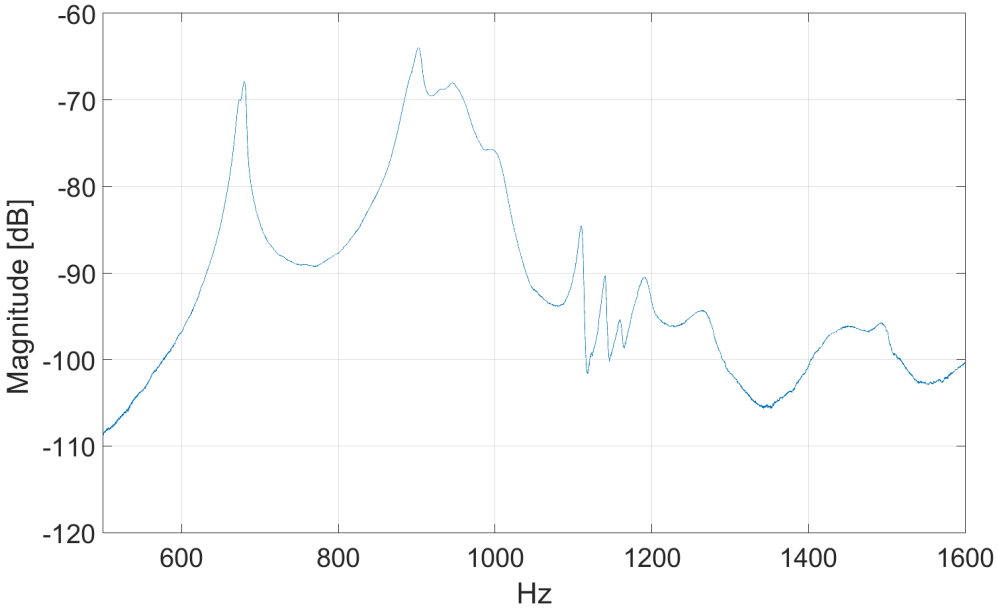

Figure 12: Average of all impacts

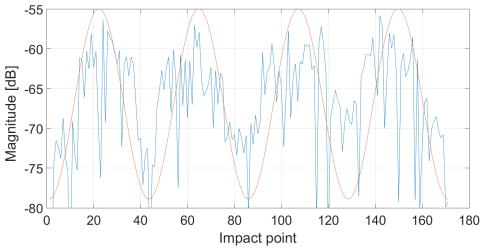

(a) 680 Hz, 2ND behaviour

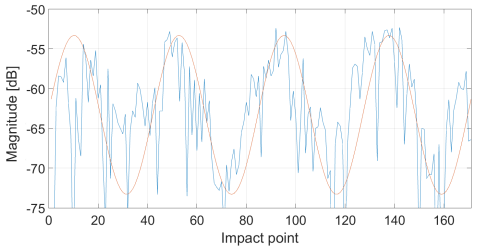

(b) 903 Hz, 2ND behaviour

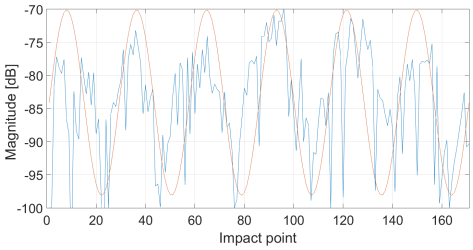

(c) 1110 Hz, 3ND behaviour

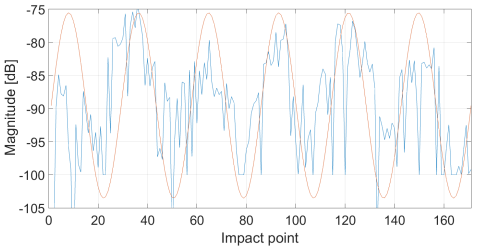

(d) 1141 Hz, 3ND behaviour

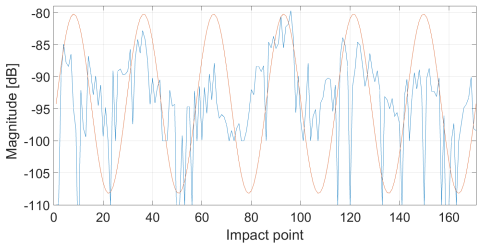

(e) 1160 Hz, 3ND behaviour

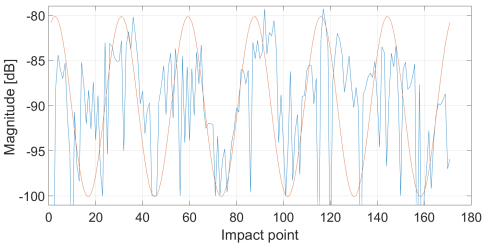

(f) 1190 Hz, 3ND behaviour

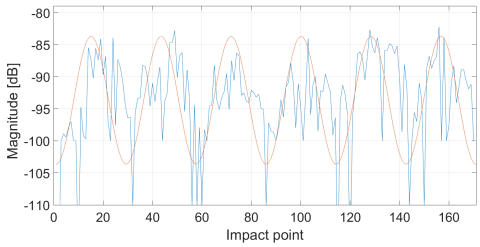

(g) 1265 Hz, 3ND behaviour

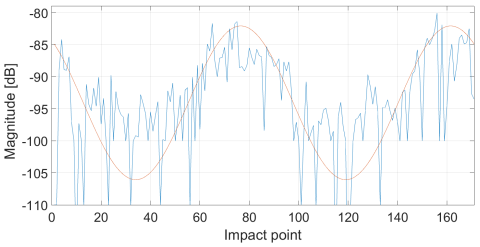

(h) 1493 Hz, 1ND behaviour

Figure 13: Results from the *impact method* of mode detection. The red line is an approximation of the amplitudes around the circumference.

The phase difference between the two sensors is calculated and transformed from angle to the number of nodal lines for each peak ($k = \frac{\Delta\alpha}{\Theta_{spatial}} \cdot \frac{360°}{2\pi}$). The nodal number k for both identification methods are presented in table 6.

Table 6: Mode identification results, in air

Frequency [Hz]	680	903	1110	1141	1160	1190	1265	1493
Phase method	2,86	2,20	2,96	2,86	2,96	2,96	2,67	0,95
Impact method	2	2	3	3	3	3	3	1

4.2.2 Improvised Impact Hammer

The presented figures in this section are FRFs, they are generated by the hammer and accelerometer signals.

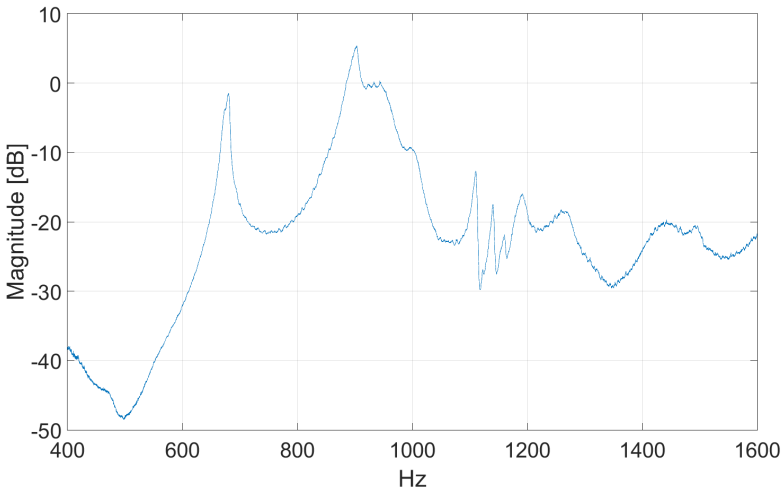

Figure 14: FRF composed by the average of all impact points in air.

The graph in figure 15 is taken from the FRF curve made up by the hammer (stimulus signal) and one accelerometer. Only the graph for the peak around 1110 Hz is presented, since the other curves are equally useless. The trend seen in figure 13 is not observed in any of the modes.

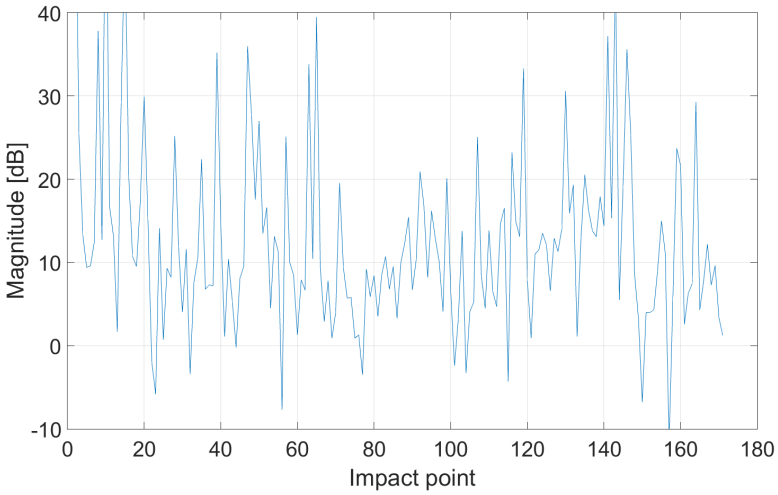

Figure 15: Result from the *impact method*. It is made up by the amplitudes in the FRF curve.

4.2.3 Submerged in water

The presented results are made by the 21 impacts. The results from the *phase identification method* is presented in table 7. The runners response is shown in figure 16.

Table 7: Phase identification method

Frequency [Hz]	430	620	682	731	960	1075	1351
Phase method	1,62	3,43	3,34	2,48	1,72	1,24	2,48

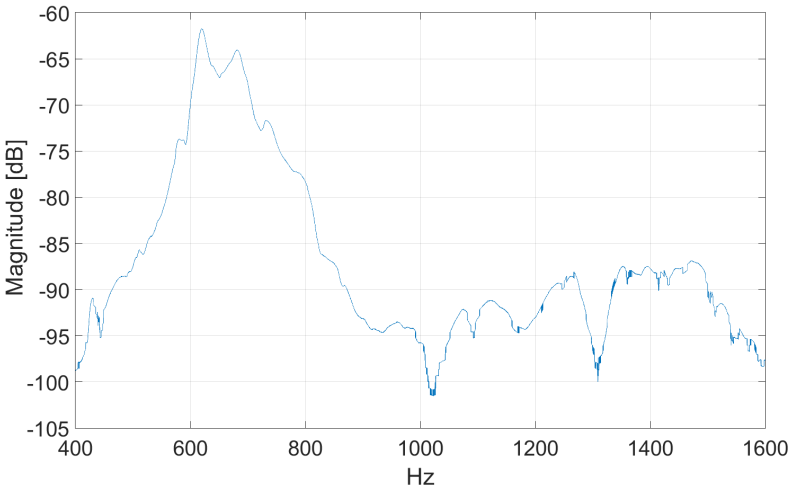

Figure 16: FFT of the average response, in water.

5 Discussion

5.1 Plate

5.1.1 Noise, stepwise sweep and impact

Truls Aarønes stated in his thesis [7] that the averaging method used to create the FRF curves for sweep excitation is theoretically wrong. This can be stated because the program divides the measurement sample into segments and creates a FRF based on each segment which span the whole frequency spectrum. Then it averages them to get a smooth curve in the end. In theory this is wrong for sweep excitation, since each segment does not contain the whole frequency range.

He generated a sweep signal that increased its frequency continuously. The differences between noise and sweep can be seen in figure 6 in [7]. This thesis uses a new sweep program with discrete frequency incrementation. If the problem was still persistent it would have manifested itself in different frequency peaks and/or damping, but since noise and sweep curves in figure 7 are identical, the problem is practically non existing.

Impact excitation has the smallest logging time, but it is interesting to notice that it gives the smoothest curve and the clearest peaks. Additionally, the frequency deviation between noise and impact excitation for the 2ND and 4ND modes is only ± 1 Hz, see table 4. Impact excitation is found to be the most reliable and the quickest method of excitation. It is therefore the preferred method for the added mass effect investigation on plates and runners.

5.1.2 Added mass and rigid surfaces

The results in section 4.1.2 clearly demonstrates that the added mass increases as the distance to a nearby rigid surface decreases and that the added mass is inversely proportional to that distance. These results are consistent with the results obtained by Valentin, see figure 1.

There are some uncertainties in these results. The plate and bottom of the tank were not parallel as the distance from the plate to the bottom varied around the circumference of the disk. The added mass is therefore not evenly distributed. How this affects the results is unknown, but the plate was twisted such that h_2 was the approximate average height. The distance directly below the accelerometer is used to calculate h_2.

The frequencies calculated by equation (11) are fairly accurate for the 2ND mode, but it underestimates the added mass for the higher modes. This tendency of underestimating the added mass was also observed in [1].

It is hard to identify correct explanations for these deviations as everything from input values, measurements and the equation itself might not be sufficiently accurate. However, the calculated frequencies show the same trend as the experimental ones.

5.2 Turbine

The identification methods
The methods did not converge to the same shape for some modes. Both methods use the same number of impact points, and thus get equally many measurements. For the impact method it does not matter if some measurements are bad, since the trend will still be evident. On the other hand, the phase method utilizes two accelerometers, and it is possible that one sensor is getting a good measurement while the other does not. If this is the case it might lead to an incorrect phase difference. However, this uncertainty is taken into account by using the median of all the differences at a given peak. By doing so, the end result should be reliable.

From this it can be seen that it is not possible to conclude on which method is the better or the more correct, both methods are equally good. Therefore if the two methods are in disagreement, it implies that the mode cannot be defined by purely diametrical nodal lines.

5.2.1 Air

In the following discussions, the phase difference is taken from table 6 and the impact method is taken from the sub figures in figure 13.

Mismatch between the identification methods
Two different methods for mode detection were used. In most cases they are in agreement, but there are larger differences in the peaks at 680 Hz and 1265 Hz.

This might indicate that these modes are not purely nodal diameters modes, they might be either torsional, flexion or modes with nodal circles. It is not possible to identify modes with these characteristics from the experiment that were conducted.

Modes with nodal circles might have been identified by impacting the turbine in the radial direction compared to impacting in the angular direction as done in my experiments. This is to be regarded as a personal theory only since the author has a limited understanding on the behaviour of these modes. The main focus in previous research papers have been on diametrical modes.

Modes at: 1110, 1141, 1160 and 1190 Hz
The observation of four modes having 3ND behaviour is unexpected. The author has not seen this in any of the reviewed papers, and has no good explanations for this phenomenon. The following is a discussion of this behaviour:

It can be assumed that the peak at 1110 Hz is the fundamental 3ND mode, since both detection methods converge to the same conclusion, and additionally this peak is the strongest of the observed 3ND modes. With this assumption it is possible to correct the value for $\Delta\theta_{Spatial}$, which then becomes 59.2 degrees[7], and not 60° as used in the calculations for phase difference. This is the reason why the phase angle is a little bit off for phase angles.

The modes at 1141, 1160 and 1190 Hz can not be harmonics of the 3ND mode, even though both detection methods implies that these are 3ND modes. Harmonics are usually observed around an integer multiple of the principle frequency, ref. results in [8][14]. This is not necessarily correct for a submerged turbine[15], but since the turbine was suspended in air this can not be the explanation.

It is possible that the peaks with lower amplitudes are caused by spectral leakage. To test this hypothesis an exponential window was applied to the measurements, but this was found not to have any effect. The peaks were still present, and no change had occurred. The sample time was eight seconds, allowing the vibrations to die before the end of the measurements. The measurement samples are therefore periodic, and no spectral leakage should be present, ref. section 2.4.3. However, it is still possible that the peaks to the right of 1110 Hz are caused by spectral leakage, although this is not likely.

Since the turbine is held together by screws, it is possible that the screws were not correctly tightened, and this might have resulted in some play between the crown/band and blades. The other peaks might arise from such a play, but this cannot be documented. However, the screws were checked and found to be correctly tightened both before and after the experiments, so it is not very likely that the peaks originates from such a possible play. Nevertheless it would be interesting to explore the influence a play like this could have on the runner response.

[7] $\Delta\theta_{spatial} = \frac{2.96 \cdot 60°}{3}$

Mode at 1493 Hz
Both identification methods converge to the same answer, and it should be safe to conclude that this is the 1ND mode.

Mode at 903 Hz
The phase difference is a bit off an integer number, and even more when correcting for the new spatial angle between the accelerometers. However, since this is the dominant peak in figure 12 and the impact method is indicating that this is a 2ND mode, it can be concluded that this is the fundamental 2ND mode.

5.2.2 Water

Identifying the modes proved to be hard because the impact method was not carried out and the phase difference between the accelerometers is useless. None of the phase differences are close to a natural number, which indicates the mode shape, except for the phase difference of the peak at 1075 Hz. This is unexpected since the test setup has not been changed from air, and the phase difference is not affected by the added mass, ref. equation (21). There were also 21 impacts which should result in a reliable median value. The phase difference for the peak at 1075 Hz cannot be trusted since the phase difference for other peaks have changed, and it might just be a coincident that the difference was close to 1.

Without any identification methods it is not possible to determine the mode shapes with certainty. But it is possible to identify one mode with the assumption that the shape of both curves in figure 12 and 16 should have similar shapes, but where the curve for water is offset to lower frequencies. In both figures there is one dominant peak which has the same shape, namely at 903 Hz in air and at 620 Hz in water. This implies that the 2ND mode has a frequency reduction ratio, $\frac{f_{water}}{f_{air}}$, of 0.68. This method of mode determination is highly speculative, and the results from using it should not be trusted.

5.2.3 Improvised impact hammer

The results from 4.2.2 partially invalidates the improvised impact hammer since no clear variation of magnitude along the impact points is observed. But the average of each impact point results in an usable FRF, ref. figure 14. The FRF is slightly more jagged compared with the pure FFT curve in figure 12, but each peak corresponds to the same frequency.

It is remarkable that the hammer method was not able to detect the variation of amplitude along the circumference of the runner, considering that both methods give curves having the same peaks. Apart from any post processing errors there are two possible causes for this. The plastic tip may provide too much damping due to the density difference between plastic and steel, which decreases the force on the hammer accelerometer. Additionally the mandrel is held by hand, and the hand will act as additional inertia resulting in a reduction of the impact force on the turbine. Both these problems can be avoided by improving the hammer design. As an example use a ball-peen hammer and make a threaded hole for mounting the accelerometer. This hammer will not experience the same damping and should not need a mandrel since the hammer ball will have a sufficiently small and hard impact area.

6 Conclusion

The aim of this thesis has been to experimentally investigate the added mass effect. Experiments have been carried out with a disk and a reversible pump turbine with the purpose of determining the relationship between added mass and distance to a nearby rigid surface. The experiments were done with the objects placed in air and with the objects submerged in water. The experiments with the disk gave good results and the added mass was found for different distances to the rigid surface. For the runner no such relationship was found.

The results from the disk experiments can be used to improve and validate numerical simulations.

Two methods have been used in the experimental modal analysis of the runner. The runner was impacted around its circumference to check how the mode amplitudes were varying, and the phase shift between two accelerometers have been used to determine the mode shapes. Two modes were identified in air, but in water the methods were not able to determine the shapes. Further experiments are needed to find the relationship between added mass and a nearby rigid surface. It is suggested to make a better impact hammer to enable better excitations of the runner.

7 Further work

A logical way to proceed this work will be to identify the modes in water to enable the determination of the added mass. It is recommended to build a better impact hammer and test different locations for placements of the accelerometers. This might be a good starting point for new experiments.

Also, it would be of great interest to investigate the effect from rotation on the natural frequencies. These experiments should be done on a simple disk to simplify the test set up.

References

[1] Valentin, D., et al., *Experimental study on the added mass and damping of a disk submerged in a partially fluid-filled tank with small radial confinement.* Journal of Fluids and Structures (2014), http://dx.doi.org/10.1016/j.jfluidstructs.2014.06.006i

[2] C.G. Rodriguez, et al., *Experimental investigation of added mass effects on a Francis turbine runner in still water.* Journal of Fluids and Structures, Pearson 2006.

[3] A.J. Wheeler, and A.R. Ganji, *Introduction to Engineering Experimentation.* 2004

[4] E. Kreyzig, *Advanced Engineering Mathematics 9th edition* Wiley 2006.

[5] Y. Kubota, *Vibration of Rotating Bladed Disc Excited by Stationary Distributed Forces.* Bulletin of the JSME, 1983. 26(221): p. 1952-1957.

[6] H. Tanaka, *Vibration behaviour and dynamic stress of runners of very high head reversiblepump-turbines.* in 15th IAHR Symposium. 1990. Belgrade.

[7] T. Aarønes, *Study of the Natural Frequencies of a Disc.* Master thesis at NTNU 2015.

[8] E. Egusquiza, et al., *Fluid added mass effect in the modal response of a pump-turbine.* Proceedings of the ASME 2009 Internation design engineering technical conferences & computers and information in engineering conference. 2009.

[9] Y. Kubota, and T. Suzuki *Added mass effect on disc vibrating in fluid.* Transactions of the Japan Society of Mechanical Engineers 50, 242-248

[10] P. Dörfler, M. Sick and A. Coutu. *Flow-Induced Pulsation and Vibration in Hydroelectric Machinery* Springer 2013.

[11] Hermod Brekke. Personal conversation, spring 2015.

[12] Peter Avitabile. *Experimental Modal Analysis, A simple Non-Mathematical Presentation.* Sound and Vibration 2001.

[13] Brian J. Schwarz, and Mark H. Richardson *Experimental Modal Analysis*, CSI Reliability Week, Orlando, FL, 1999

[14] X. Escaler, et al. *Experimental Modal Analysis of a Francis Model Runner.* in 24th IAHR Symposium in Foz, Brazil 2008.

[15] Co-supervisor Petter Østby, Rainpower. Personal conversations, spring 2015.

[16] A. Presas, et al. *On the detection of natural frequencies and mode shapes of submerged rotating disk-like structures from the casing.* Mechanical Systems and Signal Processing 60-61 547-570 (2015).

[17] Grunde Olimstad. *Characteristics of Reversible-Pump Turbines.* PhD thesis, NTNU, 2012.

[18] Einar Kobro. *Trykkpulsasjoner i Francisturbiner.* Master thesis, NTNU 2006